



HAL
open science

Selective hydroboration of terminal alkynes catalyzed by heterometallic clusters with uranium metal triple bonds

Penglong Wang, Iskander Douair, Yue Zhao, Rile Ge, Junhu Wang, Shuao Wang, Laurent Maron, Congqing Zhu

► **To cite this version:**

Penglong Wang, Iskander Douair, Yue Zhao, Rile Ge, Junhu Wang, et al.. Selective hydroboration of terminal alkynes catalyzed by heterometallic clusters with uranium metal triple bonds. *Chem*, 2022, 8 (5), pp.1361-1375. 10.1016/j.chempr.2022.03.005 . hal-03714650

HAL Id: hal-03714650

<https://hal.science/hal-03714650>

Submitted on 22 Jul 2024

HAL is a multi-disciplinary open access archive for the deposit and dissemination of scientific research documents, whether they are published or not. The documents may come from teaching and research institutions in France or abroad, or from public or private research centers.

L'archive ouverte pluridisciplinaire **HAL**, est destinée au dépôt et à la diffusion de documents scientifiques de niveau recherche, publiés ou non, émanant des établissements d'enseignement et de recherche français ou étrangers, des laboratoires publics ou privés.



Distributed under a Creative Commons Attribution - NonCommercial 4.0 International License

Article

Selective hydroboration of terminal alkynes catalyzed by heterometallic clusters with uranium–metal triple bonds

Penglong Wang,¹ Iskander Douair,² Yue Zhao,¹ Rile Ge,³ Junhu Wang,³ Shuao Wang,⁴ Laurent Maron,^{2,*} and Congqing Zhu^{1,5,*}

SUMMARY

Due to their fascinating structures and heterometallic synergistic effects in catalysis, heterometallic clusters with metal–metal (M–M) bonds have attracted the interest of chemists for decades. However, understanding of the chemistry of M–M bonds that involve f-block elements, such as uranium, is significantly less developed compared with that of the d-block transition metals, and catalysis by heterometallic clusters with U–M bonds has not been realized to date. Here, we report a set of heterometallic clusters that feature $U\equiv M$ (M = Fe, Co) triple bonds. The cluster with two $U\equiv Co$ triple bonds exhibits excellent catalytic activity for the hydroboration of alkynes under mild conditions, producing α -vinylboronates with good yields and regioselectivity. These heterometallic clusters represent the rare structurally authenticated example of multiple bonding between f-block elements and transition metals. Theoretical studies reveal high bond orders (up to 2.93) and a significant degree of covalency in these $U\equiv M$ triple bonds.

INTRODUCTION

Heterometallic clusters have considerable potential in catalysis and activation of small molecules due to the synergistic effects between different metals in close proximity.^{1–5} For instance, many metalloenzymes are thought to benefit from active sites containing more than one transition metal, which can efficiently catalyze a series of transformations.^{6–8} Compared with the extensively investigated metal–metal (M–M) bonding of transition metals, studies of M–M bonding involving actinide elements, such as uranium, are sparse.⁹ The bonding interactions of structurally authenticated U–M complexes predominantly involve single bonds^{10–22} and complexes featuring U–M multiple bonding remain relatively rare. Remarkably, a species containing a double dative bond between U and Rh was synthesized by Liddle and coworkers.²³ Moreover, Zhou, Li and coworkers reported the detection of $UFe(CO)_3^-$ and $OFe(CO)_3^-$ by mass spectroscopy in the gas phase using laser vaporization.²⁴ Computational studies show that both these complexes contain a $U\equiv Fe$ triple bond. Recently, we identified a $U\equiv Rh$ triple bond in a heterometallic cluster, which was authenticated by X-ray diffraction.²⁵ Although theoretical studies suggest that actinide–metal multiple bonding is quite common,^{26–38} no structurally authenticated species with multiple bonding between U and first-row transition metals have been isolated. Information concerning the reactivity of actinide–metal bonds is limited and the catalysis by such species has not been reported to date.

Organoboron compounds are versatile synthons in synthetic chemistry and have attracted significant attention over recent decades. The hydroboration reaction is

The bigger picture

Heterometallic synergistic effects are important in both natural metalloenzymes and synthetic chemistry and are involved in a wide variety of transformations. Although uranium is one of the most intensively investigated actinide elements, few examples of catalysis promoted by uranium complexes have been reported. In this paper, a series of heterometallic clusters with $U\equiv M$ (M = Fe, Co) triple bonds were synthesized and structurally characterized, and the cluster that contained $U\equiv Co$ triple bonds was found to be an effective catalyst for the Markovnikov-type hydroboration of alkynes with HBpin. This study supports investigation of the possibilities in catalysis and synthetic chemistry of heterometallic clusters with U–M bonds.

regarded as one of the most effective methods to construct organoboron species.^{39–41} For instance, hydroboration of alkynes is a straightforward method to construct vinylboronates, which are important synthons used in the construction of C–C bonds via a variety of coupling reactions.⁴² Although β -vinylboronates have been synthesized by the hydroboration of terminal alkynes, a reaction catalyzed by various transition metal catalysts,^{43–47} the selective synthesis of α -vinylboronates via hydroboration of terminal alkynes has been less explored.^{48–52} Therefore, the development of a new catalytic system for the direct one-step hydroboration of alkynes to α -vinylboronates is desirable.

Here, we report the first example of selective hydroboration of alkynes to α -vinylboronates catalyzed by a heterometallic cluster containing two $U\equiv Co$ triple bonds. The corresponding clusters with two $U\equiv Fe$ triple bonds were also synthesized for comparison. These structurally authenticated heterometallic molecular clusters with $U\equiv Co$ or $U\equiv Fe$ triple bonds were supported by a heptadentate N_4P_3 scaffold, and quantum chemical calculations reveal the high bond orders and significant covalency of these unusual $3d$ – $5f$ M–M triple bonds.

RESULTS AND DISCUSSION

Synthesis

Treatment of complex **1**²⁰ with $CoCl_2$ in tetrahydrofuran (THF) at room temperature (RT) causes the grayish-green suspension to turn dark-blue and the isolation of complex **2** in 46% yield after work-up (Figure 1). The 1H NMR spectrum of complex **2** exhibits a set of broad peaks spanning the range from +101.58 to –72.48 ppm (Figure S24), probably due to the presence of paramagnetic U(IV) and Co(II). After the reduction of **2** with four equivalents of KC_8 , complex **3** was isolated as dark-red crystals in a moderate and reproducible yield. Complex **3** can also be synthesized directly by the reduction of the mixture of complex **1** and $CoCl_2$ with two equivalents of KC_8 at RT (Figure 1). The 1H NMR spectrum of **3** exhibits broad resonances ranging from +72.80 to –22.71 ppm (Figure S25), which is consistent with the assignment of a U(IV) oxidation state. The differences in the 1H NMR spectra of **2** and **3** are probably due to the structural variations and the different oxidation state of Co atoms in these complexes. The formal oxidation states of the two Co atoms in complex **3** can be assigned as Co(0) given the four-electron reduction of two Co(II) in complex **2**. Complex **3** represents an unusual example of an isolated species with U–Co multiple bonds, which further demonstrates the ability of this heptadentate N_4P_3 scaffold to stabilize unusual chemical bonding.^{20,25}

In order to synthesize an analogous $U\equiv Fe$ triple bond species, two equivalents of KC_8 were added to the mixture of **1** and $FeCl_2$ in THF, which results in a dark-red suspension from which the crystalline complex **4** was isolated in 33% yield (Figure 1). The 1H NMR spectrum of complex **4** also exhibits resonances ranging from +76.57 to –44.88 ppm (Figure S27). Complexes **4** and **3** are isomorphous, except for the difference of the transition metals, and thus we proposed that this process involves an intermediate similar to complex **2** (Figure S26), which was consistent with the result of high-resolution mass spectrometry. The oxidation states of U and Fe in **4** are +IV and 0, respectively. However, in contrast to **3**, complex **4** could be further reduced by KC_8 . Treatment of crystalline **4** with two equivalents of KC_8 in THF affords complex **5** in 50% yield as dark brown crystals after recrystallization from toluene (Figure 1). Formally, the two reducing electrons in this process were used to reduce two Fe(0) to two Fe(–I), with the oxidation state of the U centers remaining unchanged. This was confirmed by the Mössbauer spectra and DFT calculations

¹State Key Laboratory of Coordination Chemistry, Jiangsu Key Laboratory of Advanced Organic Materials, School of Chemistry and Chemical Engineering, Nanjing University, Nanjing 210093, China

²LPCNO, CNRS & INSA, Université Paul Sabatier, 135 Avenue de Rangueil, 31077 Toulouse, France

³Center for Advanced Mössbauer Spectroscopy, Mössbauer Effect Data Center, Dalian Institute of Chemical Physics, Chinese Academy of Sciences, Dalian 116023, China

⁴State Key Laboratory of Radiation Medicine and Protection, School for Radiological and Interdisciplinary Sciences (RAD-X), Collaborative Innovation Center of Radiation Medicine of Jiangsu Higher Education Institutions, Soochow University, Suzhou 215123, China

⁵Lead contact

*Correspondence:
laurent.maron@irsamc.ups-tlse.fr (L.M.),
zcc@nju.edu.cn (C.Z.)

<https://doi.org/10.1016/j.chempr.2022.03.005>

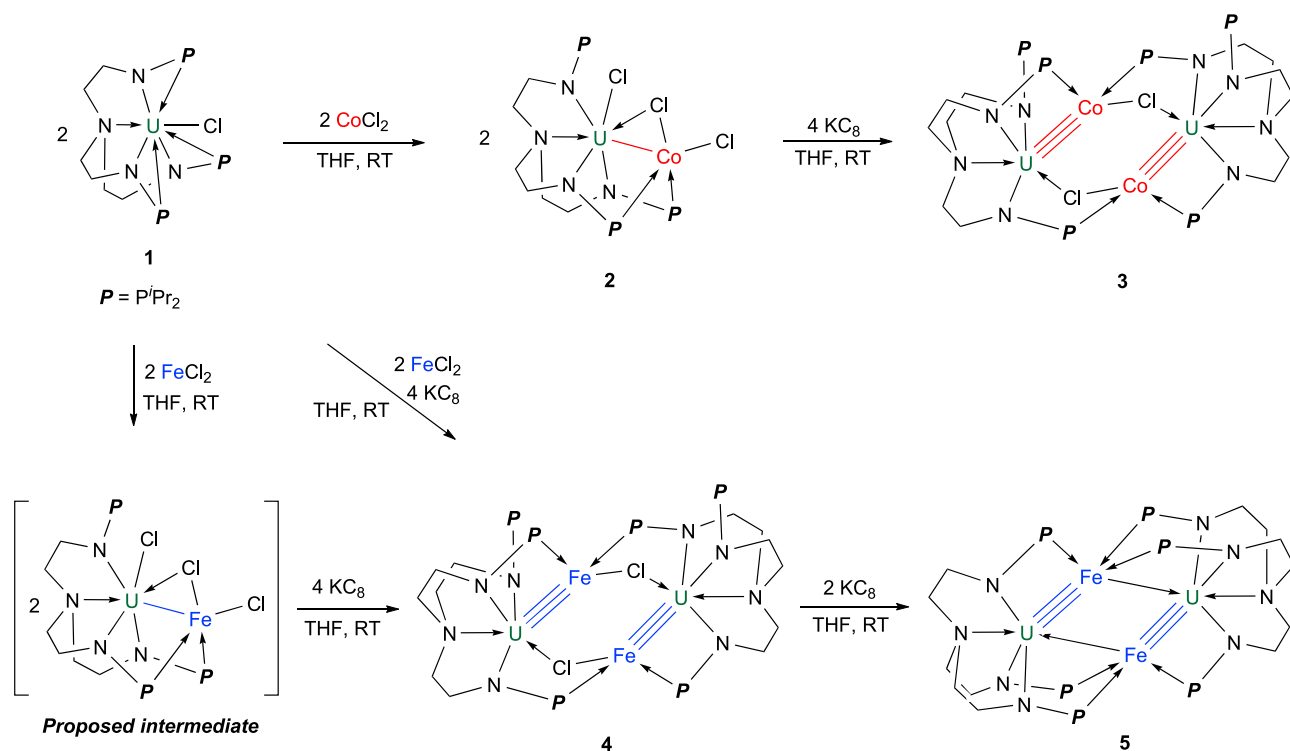


Figure 1. Synthesis of complexes 2, 3, 4, and 5 from precursor 1

The complex 3 with two $U\equiv Co$ triple bonds was formed by the reaction of KC_8 with complex 2, which was isolated from a mixture of 1 and $CoCl_2$. Reduction of the mixture of 1 and $CoCl_2$ with KC_8 affords complex 3 directly. Under similar conditions, the complex 4 containing two $U\equiv Fe$ triple bonds was prepared by the reduction of 1 and $FeCl_2$ with KC_8 . Complexes 3 and 4 are isomorphous except for the different transition metals. Treatment of complex 4 with KC_8 results in the formation of complex 5 containing two $U\equiv Fe$ triple bonds, but attempts to reduce complex 3 with KC_8 resulted in the decomposition of the reactants to unidentified products, probably because the reduction product of complex 3 is extremely unstable. RT, room temperature; THF, tetrahydrofuran.

(*vide infra*). The 1H NMR spectrum of complex 5 spans the range from +75.05 to -44.18 ppm (Figure S28). The $^{31}P\{^1H\}$ NMR spectra of 2–5 are silent between +3,000 and $-3,000$ ppm, which is probably due to the presence of paramagnetic metal ions. The isolation of complexes 3, 4, and 5 represent an example of species with a $U\equiv M$ triple bond synthesized under conventional experimental conditions.

Solid-state structures

X-ray crystallography was used to determine the solid-state structures of 2, 3, 4, and 5 (Figure 2; see also Figures S68–S71; Tables S1–S6). The $U1-Co1$ bond length of $2.9080(7)$ Å in 2 is slightly longer than the sum of the single bond covalent radii for U and Co (2.81 Å),⁵³ but it is within the previously reported range of the $U-Co$ bond distances ($2.874(3)$ – $3.0319(7)$ Å).^{13–15} The formal shortness ratio (FSR), which is defined as the ratio of the $M-M$ bond distance to the sum of the single bond covalent radii of these two metals, is a benchmark to evaluate the $M-M$ bonding because it considers the differences in the metal covalent radii. However, it is simply a qualitative index for the bonding between two metal atoms. In general, an FSR value of 1.0 indicates a single bond and a significantly smaller FSR suggests a multiple bond. The FSR value for the $U1-Co1$ in complex 2 is 1.03, very close to the FSR values for other reported $U-M$ single bonds.²⁰ The bond lengths of $U-N_{amide}$ (average of 2.229 Å) and $U-N_{amine}$ ($2.610(4)$ Å) are typical of $U(IV)$ complexes featuring this N_4P_3 ligand.²⁰

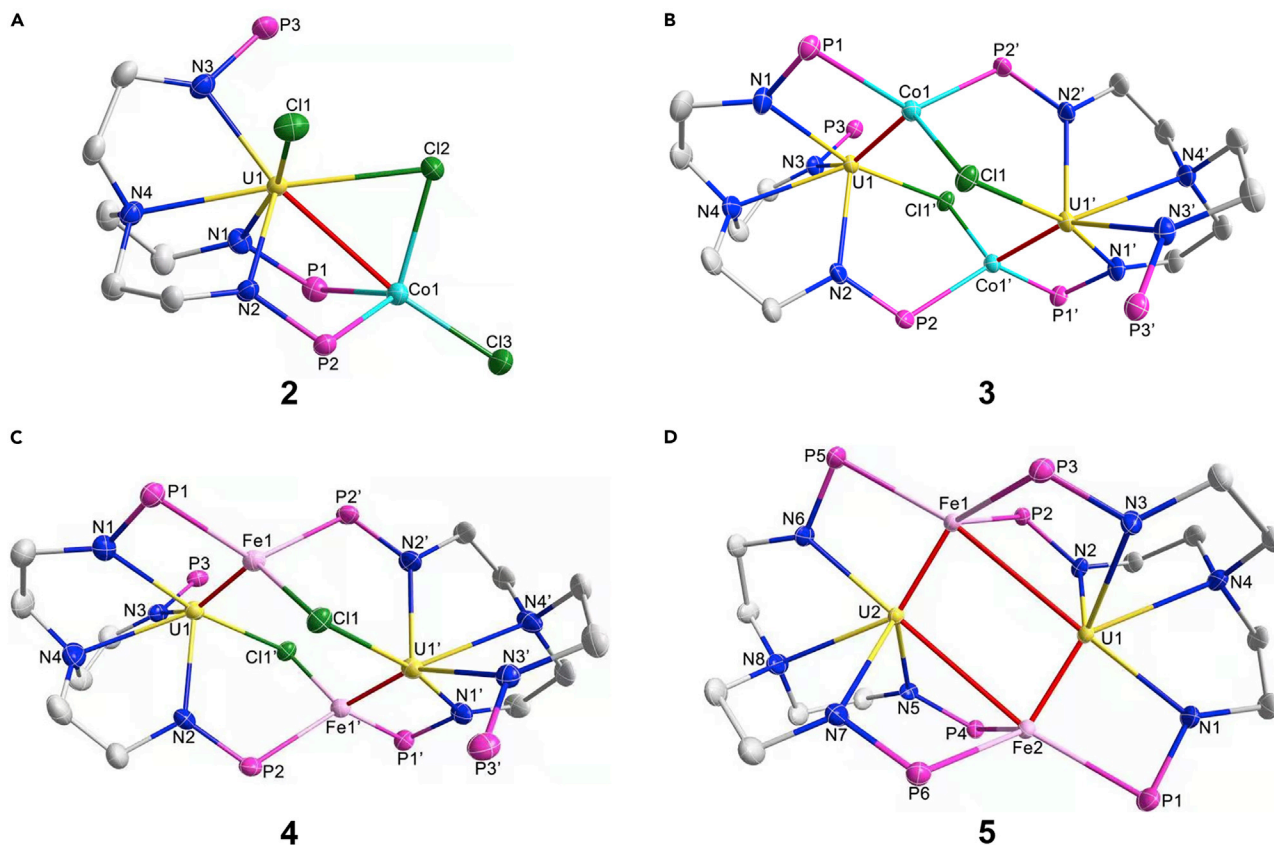


Figure 2. Molecular structures of 2, 3, 4, and 5

(A–D) Solid-state structures of 2 (A), 3 (B), 4 (C), and 5 (D) by X-ray crystallography with 50% probability ellipsoids. Hydrogen atoms, solvent molecules, and isopropyl moieties in P^iPr_2 are omitted for clarity. The U1–Co1 bond length in complex 3 (2.0854(5) Å) is shorter than the sum of the covalent triple bond radii for U and Co (2.14 Å) and significantly shorter than the U–Co bond length observed in complex 2 (2.9080(7) Å). The bond lengths of U1–Fe1 in complex 4 (1.9693(4) Å) and U1–Fe2 (2.0379(7) Å) and U2–Fe1 (2.0382(7) Å) in 5 are comparable and are all obviously shorter than the sum of the covalent triple bond radii for U and Fe (2.20 Å). The U–Co and U–Fe bonds in these species are red. Uranium, yellow; phosphorus, violet-red; nitrogen, blue; chlorine, green; cobalt, turquoise; iron, pink; and carbon, gray.

The solid-state structure of 3 exhibits a centrosymmetric dimer revealed by X-ray diffraction crystallography (Figure 2B). The U1–Co1 bond length in complex 3 (2.0854(5) Å) is much shorter than the reported U–Co bond distances in the literature (2.9450(9) Å, 3.0812(7)–2.874(3) Å, and 3.0319(7) Å),^{13–15} which is also shorter than the sum of the triple bond covalent radii for U and Co (2.14 Å).⁵⁴ Although the triple bond covalent radius of Co (0.96 Å) is only 0.1 Å less than that of Rh (1.06 Å), the U1–Co1 bond in 3 is 0.23 Å shorter than the reported U≡Rh triple bond length (2.3125(10) Å).²⁵ The FSR value for the U1–Co1 bond in 3 is 0.74, which is consistent with the FSR values for the triple bond between transition metals.⁵⁵ The extremely short U–M bond distance (2.0854(5) Å) in complex 3 suggests a strong interaction between U and Co in this species.

Complex 4 was also characterized by single-crystal X-ray diffraction analysis and revealed a centrosymmetric dimer containing two U≡Fe triple bonds (Figure 2C). The steric configurations for uranium and transition metals in complexes 3 and 4 are identical. The U1–Fe1 bond length (1.9693(4) Å) in 4 is significantly shorter than the U–Fe bond distance (2.9462(3) Å) in a previously synthesized complex.¹⁷ It is also shorter than the calculated U≡Fe triple bond lengths in $UFe(CO)_3^-$ (2.20 Å) and

$\text{OUFe}(\text{CO})_3^-$ (2.15 Å).²⁴ The U1–Fe1 bond length in **4** is 0.23 Å shorter than the sum of the covalent triple bond radii of U and Fe (2.20 Å).⁵⁴ Therefore, complex **4** has the smallest FSR value (0.69) and possesses the shortest length (1.9693(4) Å) for any structurally authenticated U–M bond, which indicates the strong multiple bonding feature between U and Fe in complex **4**.

An X-ray diffraction study of **5** exhibits the presence of a square-shaped U_2Fe_2 core structure (Figure 2D). The bond lengths of U1–Fe2 (2.0379(7) Å) and U2–Fe1 (2.0382(7) Å) in complex **5** are slightly longer than the U–Fe bond length (1.9693(4) Å) observed in **4**, which is probably due to the larger coordination numbers and steric hindrance of the Fe center in complex **5**. Nevertheless, these U–Fe distances are shorter than the predicted $\text{U}\equiv\text{Fe}$ triple bonds in $\text{UFe}(\text{CO})_3^-$ (2.20 Å) and $\text{OUFe}(\text{CO})_3^-$ (2.15 Å)²⁴, and also shorter than the sum of the covalent triple bond radii for U and Fe (2.20 Å).⁵⁴ The FSR values for U1–Fe2 and U2–Fe1 are 0.71, and are consistent with the FSR value for the U–Co multiple bonds in **3**. The bond distances for U1–Fe1 (3.1723(8) Å) and U2–Fe2 (3.1920(8) Å) are slightly longer than the sum of the covalent single bond lengths of U and Fe (2.86 Å) but are close to the U–Fe distances found in ferrocenyl-based species (3.08–3.16 Å).^{56–58} Nevertheless, complex **5** provides an example of a heterometallic cluster with two $\text{U}\equiv\text{Fe}$ triple bonds and two U–Fe single bonds. The isolation and X-ray diffraction of complexes **3**, **4**, and **5** represent the rare examples of structurally authenticated M–M multiple bonds between *f*-block elements and transition metals and also provide new opportunity to explore the properties of heterometallic clusters with U–M bonds.

UV-vis-NIR spectra

The electronic absorption spectra of **2–5** were recorded in THF at RT (Figure 3; see also Figures S12–S15). Complex **2** displays strong charge-transfer absorption in the range 300–800 nm, while **3** exhibits a broad shoulder at ~300 nm and a peak at ~408 nm. Complex **4** also exhibits broad and intense charge-transfer bands in the ultraviolet-visible (UV-vis) region with a peak centered at 557 nm. The dark-red **5** displays a largely featureless absorption spectrum in its UV-vis region. However, a series of similar and low intensity absorptions were observed in the near infrared (NIR) region (ca. 900–1,600 nm, $\epsilon = 20\text{--}350 \text{ M}^{-1} \text{ cm}^{-1}$) for these complexes, and this was attributed to the Laporte forbidden $5f \rightarrow 5f$ transitions expected for U(IV) complexes. For instance, the peaks at 1,178, 1,374, 1,393, and 1,546 nm for **3** ($\epsilon < 60 \text{ M}^{-1} \text{ cm}^{-1}$) and 1,177, 1,370, and 1,395 nm for **5** ($\epsilon < 150 \text{ M}^{-1} \text{ cm}^{-1}$) were observed in the NIR region (Figure 3). The intense absorption bands in the UV-vis region and relatively weak absorption bands in the NIR for these complexes compare well with the reported results for U(IV) complexes.^{59–61}

Mössbauer spectroscopy

To investigate the oxidation state of Fe in complexes **4** and **5**, the zero-field ^{57}Fe Mössbauer spectra of **4** and **5** were measured at 80 K on crystalline samples and feature single quadrupole doublets (Figures 4A and 4B). To the best of our knowledge, no ^{57}Fe Mössbauer data of U–Fe derivatives have been reported, thus a comparison of the isomer shift of **4** with other U–Fe systems is unavailable. The fitting isomer shift of **4** ($\delta = 0.68 \text{ mm s}^{-1}$ relative to $\alpha\text{-Fe}$ at RT) is greater than the values for M/Fe⁰ bimetallic complexes; e.g., $^i\text{PrN}=\text{Nb}(^i\text{PrNPPH}_2)_3\text{Fe}-\text{PMe}_3$ ($\delta = 0.41 \text{ mm s}^{-1}$),⁶² $\text{FeTi}(\text{N}(\text{o}-(\text{NCH}_2\text{P}^i\text{Pr}_2)\text{C}_6\text{H}_4)_3)$ ($\delta = 0.35 \text{ mm s}^{-1}$),⁶³ $\text{Cr}(^i\text{PrNPPH}_2)_3\text{Fe}-\text{PMe}_3$ ($\delta = 0.25 \text{ mm s}^{-1}$),⁶⁴ and $\text{FeV}(\text{N}(\text{o}-(\text{NCH}_2\text{P}^i\text{Pr}_2)\text{C}_6\text{H}_4)_3)$ ($\delta = 0.25 \text{ mm s}^{-1}$).⁶⁵ The greater isomer shifts of complex **4** may be attributed to the different local environments around the Fe center and the highly polarized $\text{U}\equiv\text{Fe}$ triple bond (*vide infra*).

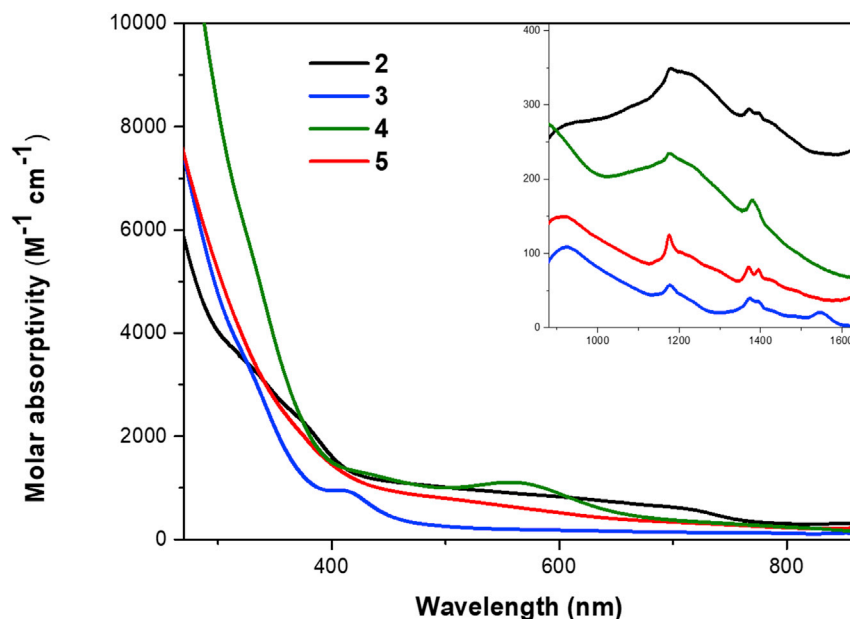


Figure 3. UV-visible absorption spectra for 2, 3, 4, and 5

The absorption spectra were measured in THF at RT. The higher molar absorption coefficients in the UV-vis region and the weak absorption bands in NIR are consistent with the data for U(IV) species. Inset: near infrared absorption spectra.

Previous studies have shown that the reduction of the Fe center results in a decrease in the fitting isomer shift.⁶² Consistently, the fitting isomer shift of 5 ($\delta = 0.55 \text{ mm s}^{-1}$) is slightly smaller than that of 4 ($\delta = 0.68 \text{ mm s}^{-1}$) (Figure 4B). The δ value of 5 is identical to that reported for the Fe(-I) complex [(CAAC)₂Fe(N₂)] [K(18-crown-6)] ($\delta = 0.56 \text{ mm s}^{-1}$).⁶⁶ These results imply that the oxidation state of the Fe center in complex 5 should be -1. The quadrupole splitting (QS) value of 5 (QS = 3.29 mm s^{-1}) is slightly larger than that of complex 4 (QS = 2.64 mm s^{-1}), which can be attributed to the different coordination spheres at the Fe centers.

Magnetic studies

The variable-temperature magnetic moments for 2, 3, 4, and 5 in the solid state (Figure 4; see also Figures S1–S11) were collected using a superconducting quantum interference device (SQUID). The data for 2 exhibit a steady drop in μ_{eff} as the temperature lowers. μ_{eff} decreases from $3.43 \mu_{\text{B}}$ at 300 K to $2.43 \mu_{\text{B}}$ at 1.8 K (Figure S1).⁶⁷ The RT moment of 2 was significantly lower than that expected for a system with one Co(II) ion and one U(IV) ion. The larger μ_{eff} of complex 2 at 1.8 K is caused mainly by the Co(II) ion as the U(IV) center is a magnetic singlet at low temperature. The magnetic moment of 3 is $3.34 \mu_{\text{B}}$ at RT, which is also lower than the sum of the expected values for ³H₄ configuration 5² U(IV) ion ($3.58 \mu_{\text{B}}$) and spin-only value for $S = \frac{1}{2} d^9$ Co(0) ion ($1.73 \mu_{\text{B}}$). The magnetic moment of complex 3 exhibits a gradual decrease upon lowering the temperature from 300 K to 25 K (Figure S3). However, at the lower temperature, complex 3 displays a slight increase in μ_{eff} , which is probably due to the weak ferromagnetic interactions.

The effective magnetic moments of 4 and 5 were found to be 3.16 and $4.26 \mu_{\text{B}}$ per molecule at 300 K (Figures 4C and 4D), respectively, which are much lower than the expected value for the sum of 5² U(IV) ion ($3.58 \mu_{\text{B}}$) and spin-only value for $S = 1 d^8$ Fe(0) ion ($2.83 \mu_{\text{B}}$) or $S = \frac{1}{2} d^9$ Fe(-I) ion ($1.73 \mu_{\text{B}}$). The smaller magnetic moments

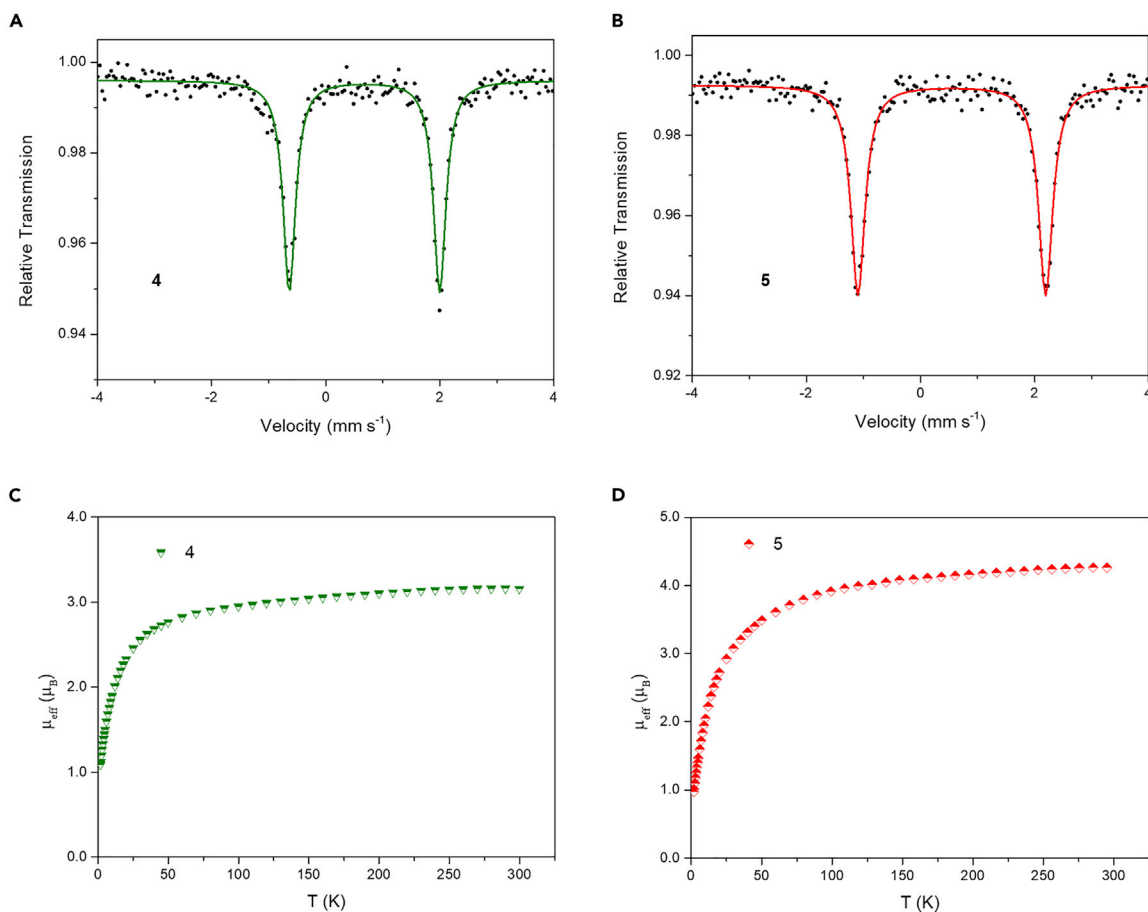


Figure 4. Mössbauer spectra and magnetic moment data of 4 and 5 on crystalline samples

(A and B) Zero-field ^{57}Fe Mössbauer spectra of 4 (A) and 5 (B) obtained at 80 K. The data (dots) and best fits (solid line) are shown. The parameters are $\delta = 0.68 \text{ mm s}^{-1}$ and $\text{QS} = 2.64 \text{ mm s}^{-1}$ for 4 and $\delta = 0.55 \text{ mm s}^{-1}$ and $\text{QS} = 3.29 \text{ mm s}^{-1}$ for 5, δ is relative to $\alpha\text{-Fe}$ at RT.

(C and D) The variable-temperature effective magnetic moment data of 4 (C) and 5 (D). The magnetic behaviors exhibit strong temperature dependency which trends to zero at low temperatures, indicating U(IV) centers in these complexes.

could be ascribed to the partial electron rearrangement between U and Fe centers, and this is supported by theoretical analysis (*vide infra*). With decreasing temperature, the magnetic moments of 4 and 5 slowly decrease to 2.76 and 3.49 μ_{B} at 50 K and drop sharply to 1.09 and 0.97 μ_{B} at 1.8 K, respectively. The curves of 4 and 5 are reminiscent of the variable-temperature magnetism of the species containing a U(IV)–Rh double dative bond reported by Liddle and coworkers.²³ The temperature dependency of magnetic moments for these complexes is consistent with a singlet ground state $5f^2$ U(IV) center with an $^3\text{H}_4$ configuration.

DFT calculations

To gain further insight into the unusual U–Co and U–Fe interactions in complexes 2–5, calculations were carried out at the DFT level (B3PW91 functional). First, the optimized geometries of the four complexes are in very good agreement with the experimentally determined geometry (see Tables S7–S10), and the U–M distances are reproduced with a maximum deviation of 0.08 Å. The bonding situation was thus analyzed with the natural bonding orbital (NBO) approach. In 2, where the U–Co bond is longer than the sum of the covalent radii, NBO analysis does not indicate any substantial bonding interaction between U and Co. However, a

Table 1. Calculated NBO compositions of the U–M natural orbitals in complexes 3, 4, and 5

	FSR _{U-M}	σ -component				π_1 -component				π_2 -component			
		M%	U%	M 3p:3d	U 7s:7p:6d:5f	M%	U%	M 3p:3d	U 7s:7p:6d:5f	M%	U%	M 3p:3d	U 7s:7p:6d:5f
3	0.74	81.27	18.73	0:99	0:2:17:80	80.67	19.33	0:99	1:12:33:53	72.64	27.40	1:99	0:6:28:66
4	0.69	85.81	14.19	0:99	3:5:30:62	84.31	15.69	0:99	0:2:17:80	82.19	17.81	0:99	1:3:25:70
5	0.71	80.34	19.66	0:99	0:6:34:58	82.70	17.30	0:99	0:1:28:70	83.72	16.28	1:96	1:1:19:78

3c–2e bond U–Cl–Co is observed, which explains the relatively low U–Co Wiberg bond index (WBI) of 0.14. Different spin states were optimized, and two spin states were found to be very close in energy, as a quartet (three unpaired electrons) and a sextet (five unpaired electrons). In both spin states, two unpaired spins are located at the uranium center, in line with a U(IV) system, while the remaining one or three unpaired spins are located at the cobalt, in line with LS or HS Co(II). Interestingly, some spin transfers from the U to the Co center (roughly 0.4 electrons), and this may explain why the observed magnetic moment is lower than the expected moment at RT. This was validated by a complete active space self-consistent field (CASSCF) calculation in which the five electrons were distributed over eight orbitals. At this level, the ground state remains a quartet but with a sextet contribution (28%), explaining the lower magnetic moment of complex 2. A similar study was carried out on complex 3. At the NBO level, two U≡Co triple bonds (Table 1) are found in complex 3. The $\sigma + 2\pi$ bonds are found to be polarized toward Co (82%–72%). The bonding interaction implies mainly the 5f of U (80% for the σ and 53%–66% for the π) and a pure 3d orbital on Co. These bonding orbitals are depicted in Figure 5A and were found to have a good proportion of covalency, as evidenced by the U–Co WBI of 2.82. The lowest energy spin state in 3 is a septet (Table S11). This spin state and the analysis of the unpaired spin values (1.62 for U and 1.38 for Co) are consistent with the presence of U(IV) and Co(0) centers. As already found for complex 2, some unpaired spin density is transferred from U(IV) to Co(0), so that the experimental magnetic moment is lower than expected. As for complex 3, this is validated by a CASSCF calculation in which six electrons are distributed over eight orbitals. The ground state at this level is a septet, with contributions from the quintet (20%) and the triplet (12%), consistent with the observed low magnetic moment.

Complex 4 also exhibits two U≡Fe triple bonds, which are strongly polarized toward Fe (82%–86%). The bonding interaction mainly involves the 5f orbitals on U (62% in the σ and 70%–80% in the π) and pure 3d on Fe (Table 1). These bonding orbitals are depicted in Figure 5B and are quite covalent (U–Fe WBI of 2.17). The WBI for the U–Fe bond in complex 4 is lower than the WBI for the U–Co bond in 3, consistent with slightly more strongly polarized bonds in 4 than in 3. Two spin states were found to be close in energy—a quintet and a nonet—both in line with a U(IV)–Fe(0) complex with Fe(0) either LS or HS. The lowest spin state is the nonet, and the unpaired spin densities on U(1.88) and Fe(2.14) are consistent with a U(IV) and a Fe(0) HS. It should be noted that once again some spin density transfer between the U and the Fe centers is occurring. As in 2 and 3, CASSCF calculations for 4 (eight electrons in eight orbitals) give rise to a nonet ground state with some contribution from the quintet (15%), consistent with the lower magnetic moment.

Finally, calculations were carried out on complex 5. Again, two U≡Fe triple bonds were found and are still strongly polarized toward Fe (80%–84%). The bonding analysis is very similar to that found in complex 4. Indeed, here the bonding interactions also involve mainly the 5f orbital on the U centers (58% for the σ and 70%–78% in the π) and pure 3d orbitals on Fe (Table 1). These bonding interactions are depicted in

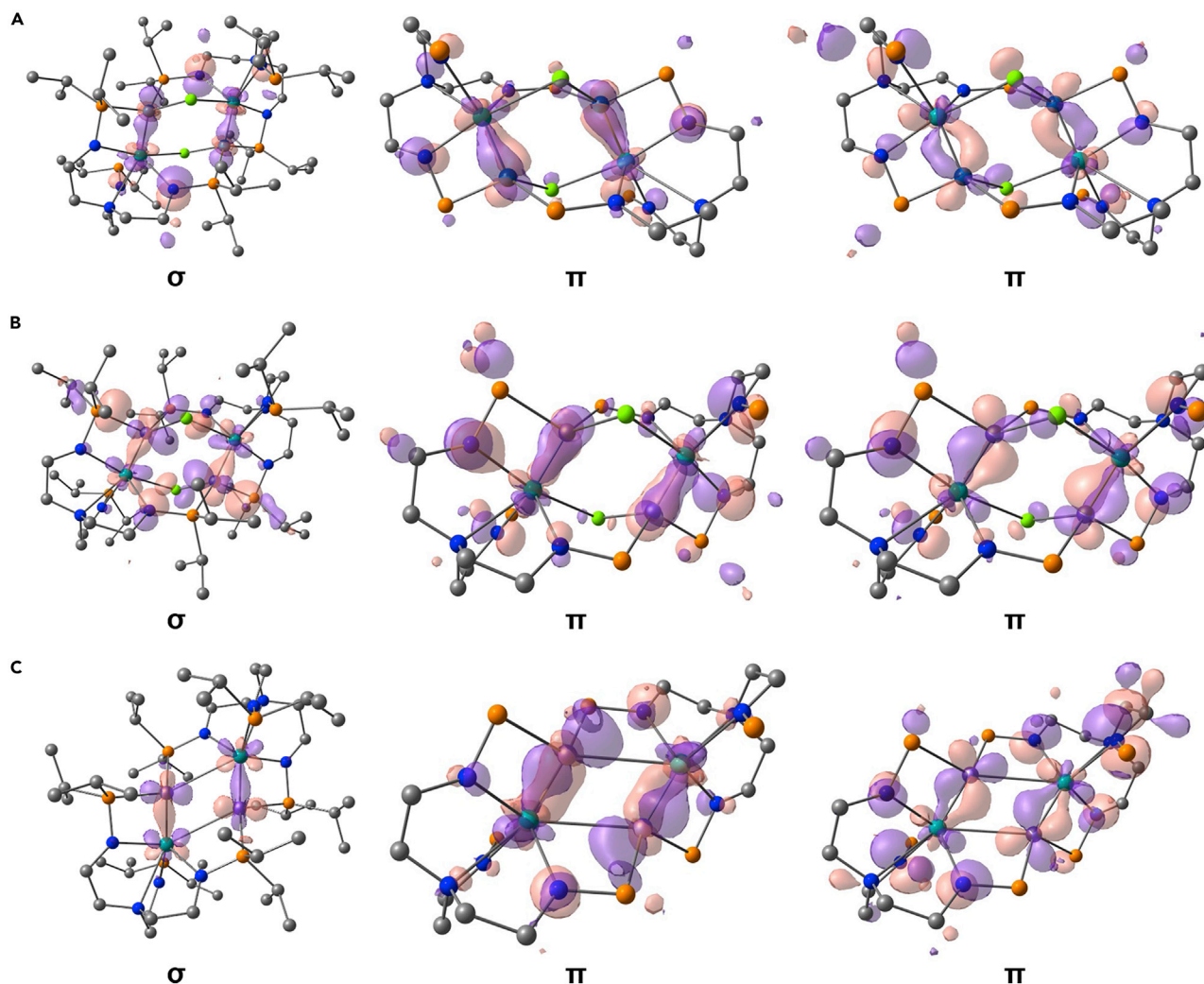


Figure 5. Bonding U-M molecular orbitals for complexes 3, 4, and 5

(A–C) 3D representations of the $U\equiv M$ triple bonds in 3 (A), 4 (B), and 5 (C). Isopropyl moieties in P^iPr_2 for the π orbitals are omitted for clarity.

Figure 5C and are strongly covalent (U–Fe WBI of 2.93). The difference in covalency between 4 and 5 could be attributed to the removal of the two U–Fe bridging chlorine atoms in 5 that allows a better overlap between the 3d orbital of Fe and the 5f orbitals of U. For this complex, the septet spin state is by far the lowest, which is consistent with a U(IV) and a Fe(I). The latter oxidation states are corroborated by the analysis of the unpaired spin densities on U(1.75) and Fe(1.25). As in all other complexes, some spin density transfer from U to Fe is observed. Again, this is corroborated by CASSCF calculations (six electrons in eight orbitals) in which the septet ground state shows a contribution from the quintet (18%).

Catalytic activity

The earth-abundant transition metals Co and Fe have been found to be efficient catalysts in hydroformylation reactions.^{41,42} Although the complexes with U–Co and U–Fe bond have been known for many years,^{10,13–15,17} no catalytic properties have been reported for these species or any other complexes with U–M bonds. With the heterometallic clusters 2, 3, 4, and 5 in hand, the catalytic activity for the hydroboration of terminal alkynes was investigated. The hydroboration experiment

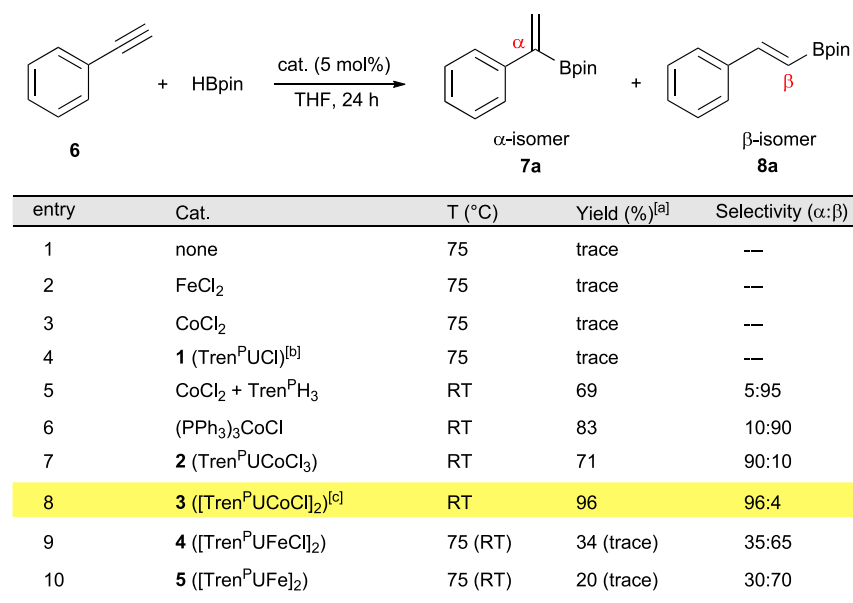


Figure 6. Screening of catalysts for alkyne hydroboration

Reaction conditions: compound **6** (0.1 mmol), HBpin (1.1 equiv), THF (1.5 mL).

^a¹H NMR yield.

^bTren^P = [N(CH₂CH₂NPⁱPr₂)₃].

^c2.5 mol% cat.

was performed using phenylacetylene as a model substrate and pinacolborane (HBpin) as the boron source (Figure 6). The CoCl₂, FeCl₂, and complex **1** were found to be inactive as catalysts for this model of hydroboration, even when reacted at 75°C for 24 h (entries 1–4). However, reactions catalyzed by the combination of CoCl₂ with Tren^PH₃ (entry 5) and (PPh₃)₃CoCl (entry 6) give rise to the formation of β -vinylboronate in good yield and selectivity. In contrast, complex **2** with a U–Co single bond formed by the reaction of complex **1** with CoCl₂, exhibits a moderate catalytic activity and produces α -vinylboronate **7a** in 71% yield (entry 7). Moreover, complex **3** with two U \equiv Co triple bonds displays excellent catalytic activity and selectivity in the formation of α -vinylboronate **7a** at RT and with a 2.5 mol% catalyst load (entry 8), which is comparable with the best result reported previously.⁵¹ No hydroboration activity was observed when either complex **4** or **5** was used at RT in this model reaction, and only poor yields and selectivity were observed at 75°C (entries 9 and 10), which is consistent with the less successful iron-catalyzed hydroboration of alkynes.⁵² These experiments show that the cooperativity between uranium and cobalt is important for the selective formation of the Markovnikov-type hydroboration product **7a** by the reaction of phenylacetylene with HBpin.

Encouraged by these initial results, we examined substrate scopes and limitations of this alkyne hydroboration catalyzed by complex **3** (Figure 7; see also Figures S29–S67). The hydroboration of phenylacetylene derivatives with electron-withdrawing substituents affords α -vinylboronates (**7b**, **7c**, **7d**, and **7e**) with good yield and regioselectivity. Electron-donating substituted phenylacetylene, e.g., *p*-methoxyphenylacetylene, could also undergo this transformation to afford α -isomer with excellent regioselectivity (**7f**). Heterocyclic alkyne derivatives (**7g** and **7h**) are also suitable substrates in this reaction, delivering α -isomers selectively in good yield. Aliphatic terminal alkynes could deliver the corresponding α -vinylboronate as major products

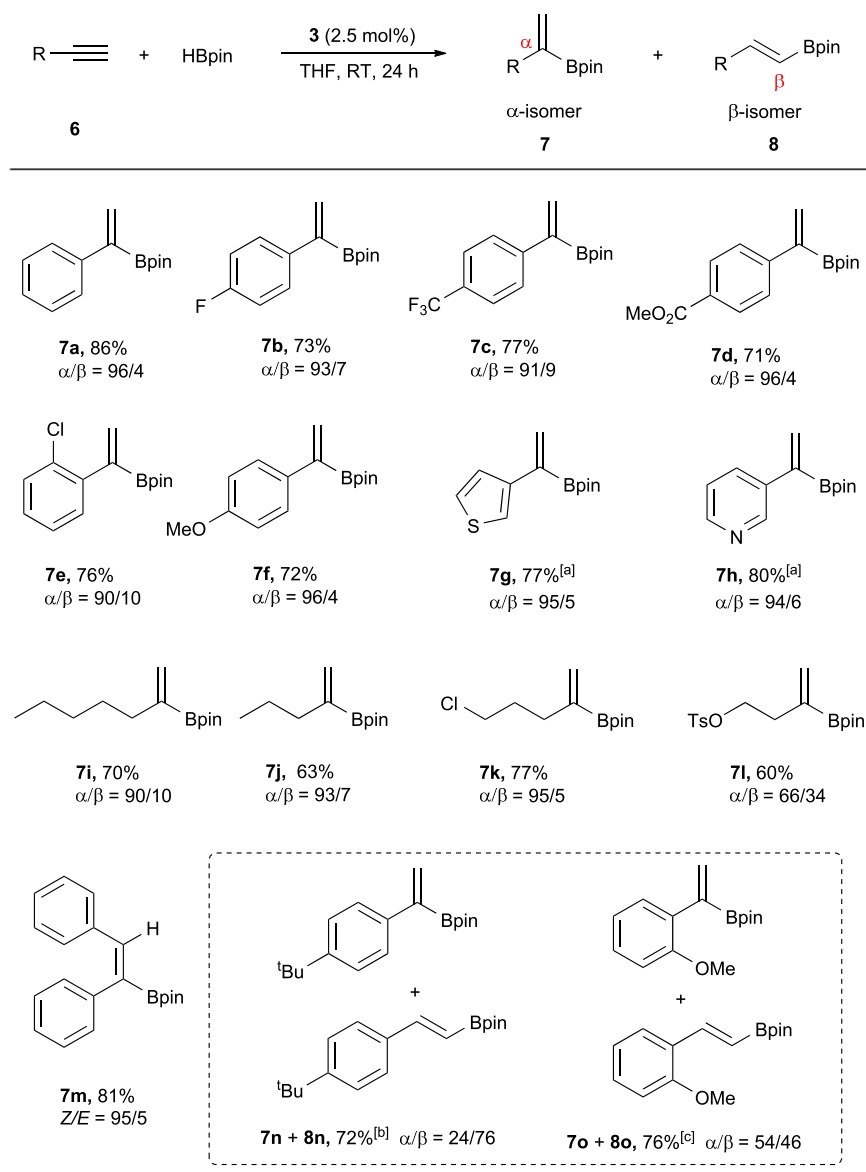


Figure 7. Scope for the hydroboration of alkynes using complex 3 as a catalyst

Yields were determined by isolated yield unless otherwise stated.

^a¹H NMR yield.

^bTotal ¹H NMR yield for α and β isomers.

^cTotal ¹H NMR yield for α and β isomers at 75°C (RT, trace).

(7i, 7j, 7k, and 7l). An internal alkyne such as diphenylacetylene, can undergo this transformation to form a Z-isomer (7m) in 81% isolated yield. However, increasing the steric bulk of the substituent groups reduced the regioselectivity. For instance, the selectivity was reversed in the case of *p*-tert-butyl substituted phenylacetylene (7n) being employed in this reaction. In addition, when *o*-methoxyphenylacetylene serves as the substrate, only trace product was observed at RT and a lower regioselectivity was obtained ($\alpha/\beta = 54/46$) at 75°C, which may be also due to the steric effect in this reaction (7o). Moreover, when complexes 2 and 3 were used as catalysts for the formation of product 7d, the α/β selectivity was 72:28 and 96:4, respectively.

This result further confirms that complex **3** with two $\text{U}\equiv\text{Co}$ triple bonds exhibits better selectivity than complex **2** for the formation of α -vinylboronate in the hydroboration of alkynes. Examples of catalytic reactions mediated by uranium complexes have appeared in recent decades.^{68–83} For example, Meyer and coworkers reported an example of uranium-mediated electrocatalytic production of H_2 from H_2O .^{76,77} Recently, Arnold and coworkers demonstrated that a dinuclear uranium complex could bind N_2 , mediating its reduction and functionalization to NH_3 .⁸⁰ This uranium complex can catalyze conversion of N_2 to a secondary silylamine. To the best of our knowledge, however, uranium-mediated hydroboration of alkynes has not been reported. Therefore, complex **3** represents the first example of a uranium species that can be used as an effective catalyst for the hydroboration of terminal alkynes with excellent Markovnikov selectivity.

Conclusions

In summary, a series of heterometallic clusters with $\text{U}\equiv\text{M}$ triple bonds have been successfully isolated by the stabilization of an effective heptadentate N_4P_3 platform. The heterometallic cluster (**3**) has two $\text{U}\equiv\text{Co}$ triple bonds and catalyzes the hydroboration of alkynes with HBpin, the first example of such a reaction achieved in uranium systems. This reaction proceeds at RT and produces Markovnikov-type hydroboration products with excellent selectivity. This is the first example of a catalytic process mediated by a heterometallic cluster with a $\text{U}-\text{M}$ bond. The isolation of these clusters with $\text{U}\equiv\text{Fe}$ and $\text{U}\equiv\text{Co}$ triple bonds represent a rare structurally authenticated example of $\text{U}-\text{M}$ multiple bonds. The presence of a $\text{U}\equiv\text{M}$ triple bond strongly polarized toward M was revealed by density functional theoretical calculations with a high covalency (WBI up to 2.93). Additionally, the bond length of $\text{U1}-\text{Fe1}$ (1.9693(4) Å) in **4** is the shortest $\text{U}-\text{M}$ bond distance revealed by X-ray diffraction to date. These results demonstrate that the multiple bonds between actinide elements and transition metals are no longer an elusive bonding motif when an effective scaffold is employed. The details of the catalytic mechanism and the scope of the regioselective functionalization of alkynes catalyzed by these heterometallic clusters deserve further investigation.

EXPERIMENTAL PROCEDURES

Resource availability

Lead contact

Further information and requests for resources should be directed to and will be fulfilled by the lead contact, Congqing Zhu (zcq@nju.edu.cn).

Materials availability

All materials generated in this study are available from the lead contact without restriction.

Data and code availability

Crystal data of **2**, **3**, **4**, and **5** have been deposited at the Cambridge Crystallographic Data Centre (CCDC) under reference numbers CCDC-2080895 (**2**), 2080896 (**3**), 2080897 (**4**), and 2080898 (**5**). These data can be obtained free of charge from the CCDC (www.ccdc.cam.ac.uk/data_request/cif).

ACKNOWLEDGMENTS

This research was supported by the National Natural Science Foundation of China (grant no. 91961116) and the Fundamental Research Funds for the Central Universities (14380262), programs for high-level entrepreneurial and innovative talents introduction of Jiangsu Province. The authors thank Dr. Tianwei Wang at Nanjing University for assistances with SQUID experiments. L.M. is a senior member of the Institut Universitaire de France. The Humboldt Foundation and the Chinese Academy of Science are acknowledged for financial support. CalMip is also gratefully acknowledged for a generous grant of computing time. We are grateful to the reviewers for their valuable comments and suggestions.

AUTHOR CONTRIBUTIONS

Conceptualization, C.Z.; experimental investigation, P.W.; X-ray crystallography, P.W. and Y.Z.; Mössbauer spectroscopy, R.G. and J.W.; calculations, L.M. and I.D.; writing—original draft, review and editing, C.Z., L.M., P.W., J.W., and S.W.; supervision, C.Z. and L.M.

DECLARATION OF INTERESTS

The authors declare no competing interests.

Received: June 8, 2021

Revised: August 26, 2021

Accepted: March 3, 2022

Published: March 28, 2022

REFERENCES

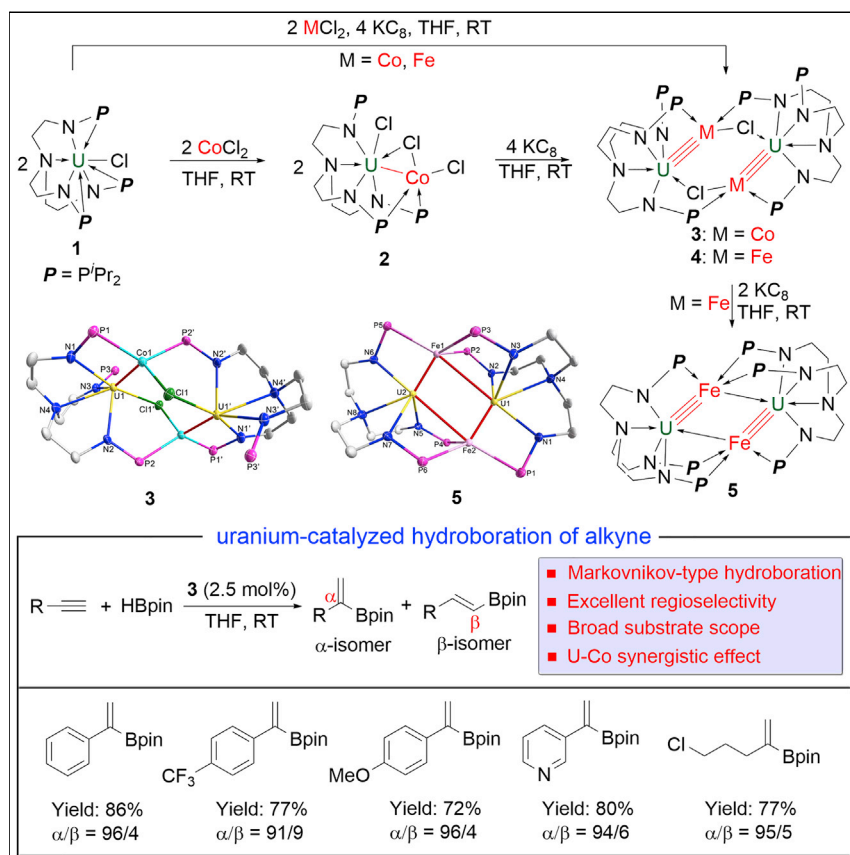
- Adams, R.D., and Cotton, F.A. (1998). *Catalysis by Di- and Polynuclear Metal Cluster Complexes* (Wiley-VCH Verlag).
- F.A. Cotton, C.A. Murillo, and R.A. Walton, eds. (2005). *Multiple Bonds Between Metal Atoms*. (Springer Science & Business Media, Inc., New York).
- Shima, T., Hu, S., Luo, G., Kang, X., Luo, Y., and Hou, Z. (2013). Dinitrogen cleavage and hydrogenation by a trinuclear titanium polyhydride complex. *Science* 340, 1549–1552.
- Hu, S., Shima, T., and Hou, Z. (2014). Carbon–carbon bond cleavage and rearrangement of benzene by a trinuclear titanium hydride. *Nature* 512, 413–415.
- McWilliams, S.F., and Holland, P.L. (2015). Dinitrogen binding and cleavage by multinuclear iron complexes. *Acc. Chem. Res.* 48, 2059–2065.
- Lindahl, P.A. (2012). Metal–metal bonds in biology. *J. Inorg. Biochem.* 106, 172–178.
- Lubitz, W., Ogata, H., Rüdiger, O., and Reijerse, E. (2014). Hydrogenases. *Chem. Rev.* 114, 4081–4148.
- W. Weigand, and P. Schollhammer, eds. (2015). *Bioinspired Catalysis* (Wiley-VCH Verlag).
- Liddle, S.T. (2015). *Molecular Metal–Metal Bonds: Compounds, Synthesis, Properties* (Wiley-VCH Verlag).
- Sternal, R.S., and Marks, T.J. (1987). Actinide-to-transition metal bonds. Synthesis, characterization, and properties of metal–metal bonded systems having the tris(cyclopentadienyl) actinide fragment. *Organometallics* 6, 2621–2623.
- Gardner, B.M., McMaster, J., Lewis, W., and Liddle, S.T. (2009). Synthesis and structure of $[(N(CH_2CH_2NSiMe_3)_3)URe(\eta^5-C_5H_5)_2]$: a heterobimetallic complex with an unsupported uranium–rhenium bond. *Chem. Commun.* 20, 2851–2853.
- Patel, D., King, D.M., Gardner, B.M., McMaster, J., Lewis, W., Blake, A.J., and Liddle, S.T. (2011). Structural and theoretical insights into the perturbation of uranium–rhenium bonds by dative Lewis base ancillary ligands. *Chem. Commun. (Camb)* 47, 295–297.
- Patel, D., Moro, F., McMaster, J., Lewis, W., Blake, A.J., and Liddle, S.T. (2011). A formal high oxidation state inverse-sandwich diuranium complex: a new route to f-block–metal bonds. *Angew. Chem. Int. Ed. Engl.* 50, 10388–10392.
- Napoline, J.W., Kraft, S.J., Matson, E.M., Fanwick, P.E., Bart, S.C., and Thomas, C.M. (2013). Tris(phosphinoamide)-supported uranium–cobalt heterobimetallic complexes featuring Co→U dative interactions. *Inorg. Chem.* 52, 12170–12177.
- Ward, A.L., Lukens, W.W., Lu, C.C., and Arnold, J. (2014). Photochemical route to actinide-transition metal bonds: synthesis, characterization and reactivity of a series of thorium and uranium heterobimetallic complexes. *J. Am. Chem. Soc.* 136, 3647–3654.
- Hlina, J.A., Pankhurst, J.R., Kaltsoyannis, N., and Arnold, P.L. (2016). Metal–metal bonding in uranium-group 10 complexes. *J. Am. Chem. Soc.* 138, 3333–3345.
- Fortier, S., Aguilar-Calderón, J.R., Vlasisavljevich, B., Metta-Magaña, A.J., Goos, A.G., and Botez, C.E. (2017). An N-tethered uranium(III) arene complex and the synthesis of an unsupported U–Fe bond. *Organometallics* 36, 4591–4599.
- Hlina, J.A., Wells, J.A.L., Pankhurst, J.R., Love, J.B., and Arnold, P.L. (2017). Uranium rhodium bonding in heterometallic complexes. *Dalton Trans.* 46, 5540–5545.
- Lu, J.B., Ma, X.L., Wang, J.Q., Jiang, Y.F., Li, Y., Hu, H.S., Xiao, H., and Li, J. (2019). The $df-d$ dative bonding in a uranium–cobalt heterobimetallic complex for efficient nitrogen fixation. *Inorg. Chem.* 58, 7433–7439.
- Feng, G., Zhang, M., Shao, D., Wang, X., Wang, S., Maron, L., and Zhu, C. (2019). Transition-metal-bridged bimetallic clusters with multiple uranium–metal bonds. *Nat. Chem.* 11, 248–253.
- Xin, X., Douair, I., Zhao, Y., Wang, S., Maron, L., and Zhu, C. (2020). Dinitrogen cleavage by a heterometallic cluster featuring multiple uranium–rhodium bonds. *J. Am. Chem. Soc.* 142, 15004–15011.
- Feng, G., McCabe, K.N., Wang, S., Maron, L., and Zhu, C. (2020). Construction of heterometallic clusters with multiple uranium–metal bonds by using dianionic

- nitrogen–phosphorus ligands. *Chem. Sci.* **11**, 7585–7592.
23. Lu, E., Wooles, A.J., Gregson, M., Cobb, P.J., and Liddle, S.T. (2018). A very short uranium(IV)–rhodium(I) bond with net double-dative bonding character. *Angew. Chem. Int. Ed. Engl.* **57**, 6587–6591.
24. Chi, C., Wang, J.Q., Qu, H., Li, W.L., Meng, L., Luo, M., Li, J., and Zhou, M. (2017). Preparation and characterization of uranium–iron triple-bonded $UFe(CO)_3$ – and $OuFe(CO)_3$ – complexes. *Angew. Chem. Int. Ed.* **56**, 6932–6936.
25. Feng, G., Zhang, M., Wang, P., Wang, S., Maron, L., and Zhu, C. (2019). Identification of a uranium–rhodium triple bond in a heterometallic cluster. *Proc. Natl. Acad. Sci. USA* **116**, 17654–17658.
26. Gagliardi, L., and Pyykkö, P. (2004). Theoretical search for very short metal–actinide bonds: NUlr and isoelectronic systems. *Angew. Chem. Int. Ed. Engl.* **43**, 1573–1576.
27. Gagliardi, L., and Roos, B.O. (2005). Quantum chemical calculations show that the uranium molecule U_2 has a quintuple bond. *Nature* **433**, 848–851.
28. Gagliardi, L., Pyykkö, P., and Roos, B.O. (2005). A very short uranium–uranium bond: the predicted metastable U_2^{2+} . *Phys. Chem. Chem. Phys.* **7**, 2415–2417.
29. Straka, M., and Pyykkö, P. (2005). Linear HThThH: a candidate for a Th–Th triple bond. *J. Am. Chem. Soc.* **127**, 13090–13091.
30. Roos, B.O., and Gagliardi, L. (2006). Quantum chemistry predicts multiply bonded diuranium compounds to be stable. *Inorg. Chem.* **45**, 803–807.
31. La Macchia, G., Brynda, M., and Gagliardi, L. (2006). Quantum chemical calculations predict the diphenyl diuranium compound $[PhUUPh]$ to have a stable 1A_g ground state. *Angew. Chem. Int. Ed. Engl.* **45**, 6210–6213.
32. Roos, B.O., Malmqvist, P.A., and Gagliardi, L. (2006). Exploring the actinide–actinide bond: theoretical studies of the chemical bond in Ac_2 , Th_2 , Pa_2 , and U_2 . *J. Am. Chem. Soc.* **128**, 17000–17006.
33. Ruipérez, F., Merino, G., Ugalde, J.M., and Infante, I. (2013). Molecules with high bond orders and ultrashort bond lengths: CrU, MoU, and WU. *Inorg. Chem.* **52**, 2838–2843.
34. Wang, C.Z., Gibson, J.K., Lan, J.H., Wu, Q.Y., Zhao, Y.L., Li, J., Chai, Z.F., and Shi, W.Q. (2015). Actinide (An = Th–Pu) dimetalloenes: promising candidates for metal–metal multiple bonds. *Dalton Trans.* **44**, 17045–17053.
35. Hu, H.S., and Kaltsoyannis, N. (2017). The shortest Th–Th distance from a new type of quadruple bond. *Phys. Chem. Chem. Phys.* **19**, 5070–5076.
36. Hu, S.X., Lu, E., and Liddle, S.T. (2019). Prediction of high bond-order metal–metal multiple-bonds in heterobimetallic 3d–4f/5f complexes $[TM–M(N(o-INC_2H_2P(CH_3)_2)_2C_6H_4)_3]$ (TM = Cr, Mn, Fe; M = U, Np, Pu, and Nd). *Dalton Trans.* **48**, 12867–12879.
37. Sharma, P., Pahls, D.R., Ramirez, B.L., Lu, C.C., and Gagliardi, L. (2019). Multiple bonds in uranium–transition metal complexes. *Inorg. Chem.* **58**, 10139–10147.
38. Knecht, S., Jensen, H.J.A., and Saue, T. (2019). Relativistic quantum chemical calculations show that the uranium molecule U_2 has a quadruple bond. *Nat. Chem.* **11**, 40–44.
39. Obligacion, J.V., and Chirik, P.J. (2018). Earth-abundant transition metal catalysts for alkene hydrosilylation and hydroboration: Opportunities and Assessments. *Nat. Rev. Chem.* **2**, 15–34.
40. Chen, J., Guo, J., and Lu, Z. (2018). Recent advances in hydrometallation of alkenes and alkynes via the first row transition metal catalysis. *Chin. J. Chem.* **36**, 1075–1109.
41. Wen, H., Liu, G., and Huang, Z. (2019). Recent advances in tridentate iron and cobalt complexes for alkene and alkyne hydrofunctionalizations. *Coord. Chem. Rev.* **386**, 138–153.
42. Ai, W., Zhong, R., Liu, X., and Liu, Q. (2019). Hydride transfer reactions catalyzed by cobalt complexes. *Chem. Rev.* **119**, 2876–2953.
43. Ohmura, T., Yamamoto, Y., and Miyaura, N. (2000). Rhodium- or iridium-catalyzed trans-hydroboration of terminal alkynes, giving (Z)-1-alkenylboron compounds. *J. Am. Chem. Soc.* **122**, 4990–4991.
44. Gunanathan, C., Hölscher, M., Pan, F., and Leitner, W. (2012). Ruthenium catalyzed hydroboration of terminal alkynes to Z-vinylboronates. *J. Am. Chem. Soc.* **134**, 14349–14352.
45. Obligacion, J.V., Neely, J.M., Yazdani, A.N., Pappas, I., and Chirik, P.J. (2015). Cobalt catalyzed Z-selective hydroboration of terminal alkynes and elucidation of the origin of selectivity. *J. Am. Chem. Soc.* **137**, 5855–5858.
46. Gorgas, N., Alves, L.G., Stöger, B., Martins, A.M., Veiros, L.F., and Kirchner, K. (2017). Stable, yet highly reactive nonclassical iron(II) polyhydride pincer complexes: Z-selective dimerization and hydroboration of terminal alkynes. *J. Am. Chem. Soc.* **139**, 8130–8133.
47. Wang, Y., Guan, R., Sivaguru, P., Cong, X., and Bi, X. (2019). Silver-catalyzed anti-Markovnikov hydroboration of C–C multiple bonds. *Org. Lett.* **21**, 4035–4038.
48. Jang, H., Zhugralin, A.R., Lee, Y., and Hoveyda, A.H. (2011). Highly selective methods for synthesis of internal (α -) vinylboronates through efficient NHC–Cu-catalyzed hydroboration of terminal alkynes. Utility in chemical synthesis and mechanistic basis for selectivity. *J. Am. Chem. Soc.* **133**, 7859–7871.
49. Yoshida, H., Takemoto, Y., and Takaki, K. (2014). A masked diboron in Cu-catalyzed borylation reaction: highly regioselective formal hydroboration of alkynes for synthesis of branched alkenylborons. *Chem. Commun. (Camb)* **50**, 8299–8302.
50. Ojha, D.P., and Prabhu, K.R. (2016). Pd-catalyzed hydroborylation of alkynes: A ligand controlled regioselectivity switch for the synthesis of α - or β -vinylboronates. *Org. Lett.* **18**, 432–435.
51. Chen, J., Shen, X., and Lu, Z. (2021). Cobalt-catalyzed Markovnikov-type selective hydroboration of terminal alkynes. *Angew. Chem. Int. Ed. Engl.* **60**, 690–694.
52. Bose, S.K., Mao, L., Kuehn, L., Radius, U., Nekkinda, J., Santos, W.L., Westcott, S.A., Steel, P.G., and Marder, T.B. (2021). First-row d-block element-catalyzed carbon–boron bond formation and related processes. *Chem. Rev.* **121**, 13238–13341.
53. Pyykkö, P. (2015). Additive covalent radii for single-, double-, and triple-bonded molecules and tetrahedrally bonded crystals: A summary. *J. Phys. Chem. A* **119**, 2326–2337.
54. Pyykkö, P., Riedel, S., and Patzschke, M. (2005). Triple-bond covalent radii. *Chemistry* **11**, 3511–3520.
55. Cotton, F.A., Matonic, J.H., and Murillo, C.A. (1997). A new type of divalent niobium compound: the first Nb–Nb triple bond in a tetragonal lantern environment. *J. Am. Chem. Soc.* **119**, 7889–7890.
56. Bucaille, A., Le Borgne, T., Ephritikhine, M., and Daran, J.C. (2000). Synthesis and x-ray crystal structure of a urana[1]ferrocenophane, the first tris(1,1'-ferrocenylene) metal compound. *Organometallics* **19**, 4912–4914.
57. Monreal, M.J., Carver, C.T., and Diaconescu, P.L. (2007). Redox processes in a uranium bis(1,1'-diamidoferrocene) complex. *Inorg. Chem.* **46**, 7226–7228.
58. Monreal, M.J., and Diaconescu, P.L. (2008). A weak interaction between iron and uranium in uranium alkyl complexes supported by ferrocene diamide ligands. *Organometallics* **27**, 1702–1706.
59. Castro-Rodríguez, I., and Meyer, K. (2006). Small molecule activation at uranium coordination complexes: control of reactivity via molecular architecture. *Chem. Commun. (Camb)* **13**, 1353–1368.
60. Wang, P., Douair, I., Zhao, Y., Wang, S., Zhu, J., Maron, L., and Zhu, C. (2021). Facile dinitrogen and dioxygen cleavage by a uranium(III) complex: cooperativity between the non-innocent ligand and the uranium center. *Angew. Chem. Int. Ed. Engl.* **60**, 473–479.
61. Liddle, S.T. (2015). The renaissance of non-aqueous uranium chemistry. *Angew. Chem. Int. Ed. Engl.* **54**, 8604–8641.
62. Culcu, G., Iovan, D.A., Krogman, J.P., Wilding, M.J.T., Bezpalko, M.W., Foxman, B.M., and Thomas, C.M. (2017). Heterobimetallic complexes comprised of Nb and Fe: isolation of a coordinatively unsaturated Nb^{III}/Fe^0 bimetallic complex featuring a $Nb\equiv Fe$ triple bond. *J. Am. Chem. Soc.* **139**, 9627–9636.
63. Eisenhart, R.J., Clouston, L.J., and Lu, C.C. (2015). Configuring bonds between first-row transition metals. *Acc. Chem. Res.* **48**, 2885–2894.
64. Kuppaswamy, S., Bezpalko, M.W., Powers, T.M., Wilding, M.J.T., Brozek, C.K., Foxman, B.M., and Thomas, C.M. (2014). A series of C3-symmetric heterobimetallic Cr–M (M = Fe, Co and Cu) complexes. *Chem. Sci.* **5**, 1617–1626.
65. Clouston, L.J., Bernales, V., Cammarota, R.C., Carlson, R.K., Bill, E., Gagliardi, L., and Lu, C.C.

- (2015). Heterobimetallic complexes that bond vanadium to iron, cobalt, and nickel. *Inorg. Chem.* **54**, 11669–11679.
66. Ung, G., and Peters, J.C. (2015). Low-temperature N₂ binding to two-coordinate L₂Fe⁰ enables reductive trapping of L₂FeN₂⁻ and NH₃ generation. *Angew. Chem. Int. Ed. Engl.* **54**, 532–535.
67. Kindra, D.R., and Evans, W.J. (2014). Magnetic susceptibility of uranium complexes. *Chem. Rev.* **114**, 8865–8882.
68. Fagan, P.J., Manriquez, J.M., Maatta, E.A., Seyam, A.M., and Marks, T.J. (1981). Synthesis and properties of bis-(pentamethylcyclopentadienyl) actinide hydrocarbyls and hydrides. A new class of highly reactive f-element organometallic compounds. *J. Am. Chem. Soc.* **103**, 6650–6667.
69. Straub, T., Haskel, A., and Eisen, M.S. (1995). Organoactinide-catalyzed oligomerization of terminal acetylenes. *J. Am. Chem. Soc.* **117**, 6364–6365.
70. Stubbert, B.D., and Marks, T.J. (2007). Constrained geometry organoactinides as versatile catalysts for the intramolecular hydroamination/cyclization of primary and secondary amines having diverse tethered C–C unsaturation. *J. Am. Chem. Soc.* **129**, 4253–4271.
71. Fox, A.R., Bart, S.C., Meyer, K., and Cummins, C.C. (2008). Towards uranium catalysts. *Nature* **455**, 341–349.
72. Gardner, B.M., Stewart, J.C., Davis, A.L., McMaster, J., Lewis, W., Blake, A.J., and Liddle, S.T. (2012). Homologation and functionalization of carbon monoxide by a recyclable uranium complex. *Proc. Natl. Acad. Sci. USA* **109**, 9265–9270.
73. Karmel, I.S.R., Tamm, M., and Eisen, M.S. (2015). Actinide-mediated catalytic addition of E–H bonds (E = N, P, S) to carbodiimides, isocyanates, and isothiocyanates. *Angew. Chem. Int. Ed.* **54**, 12599–12602.
74. Monsigny, L., Thuéry, P., Berthet, J.C., and Cantat, T. (2016). Breaking CO bonds with uranium: uranyl complexes as selective catalysts in the hydrosilylation of aldehydes. *ACS Catal.* **9**, 9025–9033.
75. West, J.G., Bedell, T.A., and Sorensen, E.J. (2016). The uranyl cation as a visible-light photocatalyst for C(sp³)–H fluorination. *Angew. Chem. Int. Ed.* **55**, 8923–8927.
76. Halter, D.P., Heinemann, F.W., Bachmann, J., and Meyer, K. (2016). Uranium-mediated electrocatalytic dihydrogen production from water. *Nature* **530**, 317–321.
77. Halter, D.P., Heinemann, F.W., Maron, L., and Meyer, K. (2018). The role of uranium–arene bonding in H₂O reduction catalysis. *Nat. Chem.* **10**, 259–267.
78. Tsoureas, N., Maron, L., Kilpatrick, A.F.R., Layfield, R.A., and Cloke, F.G.N. (2020). Ethene activation and catalytic hydrogenation by a low-valent uranium pentalene complex. *J. Am. Chem. Soc.* **142**, 89–92.
79. Li, Y., Rizvi, S.A.E.A., Hu, D., Sun, D., Gao, A., Zhou, Y., Li, J., and Jiang, X. (2019). Selective late-stage oxygenation of sulfides with ground-state oxygen by uranyl photocatalysis. *Angew. Chem. Int. Ed.* **131**, 13633–13640.
80. Arnold, P.L., Ochiai, T., Lam, F.Y.T., Kelly, R.P., Seymour, M.L., and Maron, L. (2020). Metallacyclic actinide catalysts for dinitrogen conversion to ammonia and secondary amines. *Nat. Chem.* **12**, 654–659.
81. Hu, D., Zhou, Y., and Jiang, X. (2021). From aniline to phenol: carbon-nitrogen bond activation via uranyl photoredox catalysis. *Natl. Sci. Rev.* <https://doi.org/10.1093/nsr/nwab156>.
82. Makarov, K., Kaushansky, A., and Eisen, M.S. (2022). Catalytic hydroboration of esters by versatile thorium and uranium amide complexes. *ACS Catal.* **12**, 273–284.
83. Hartline, D.R., and Meyer, K. (2021). From chemical curiosities and trophy molecules to uranium-based catalysis: developments for uranium catalysis as a new facet in molecular uranium chemistry. *JACS Au* **1**, 698–709.

Article

Selective hydroboration of terminal alkynes catalyzed by heterometallic clusters with uranium–metal triple bonds



Understanding of the chemistry of M–M bonds that involve *f*-block elements is significantly less developed compared with that of the *d*-block transition metals, and the catalysis by heterometallic clusters with U–M bonds has not been realized. Herein, Wang et al. describe the selective hydroboration of terminal alkynes catalyzed by heterometallic clusters with uranium–cobalt triple bonds under mild conditions, producing α -vinylboronates with good yields and regioselectivity.

Penglong Wang, Iskander Douair, Yue Zhao, ..., Shuao Wang, Laurent Maron, Congqing Zhu

laurent.maron@irsamc.ups-tlse.fr (L.M.)
zcq@nju.edu.cn (C.Z.)

Highlights

Uranium-catalyzed selective hydroboration of alkynes

Catalytic reaction promoted by a cluster with U–M bonds

Heterometallic molecular clusters with U≡M triple bonds

The shortest U–M bond (1.9693(4) Å) revealed by X-ray diffraction